DOT/FAA/TC-25/23

Federal Aviation Administration
William J. Hughes Technical Center
Aviation Research Division
Atlantic City International Airport
New Jersey 08405

Implementation of Thick-Shell Finite Elements in the MAT_213 Composite Material Model in LS-DYNA

January 2026

Final report

U.S. Department of Transportation
Federal Aviation Administration

NOTICE

This document is disseminated under the sponsorship of the U.S. Department of Transportation in the interest of information exchange. The U.S. Government assumes no liability for the contents or use thereof. The U.S. Government does not endorse products or manufacturers. Trade or manufacturers' names appear herein solely because they are considered essential to the objective of this report. The findings and conclusions in this report are those of the author(s) and do not necessarily represent the views of the funding agency. This document does not constitute FAA policy. Consult the FAA sponsoring organization listed on the Technical Documentation page as to its use.

This report is available at the Federal Aviation Administration William J. Hughes Technical Center's Full-Text Technical Reports page: actlibrary.tc.faa.gov in Adobe Acrobat portable document format (PDF).

Technical Report Documentation Page

Form DOT F 1700.7 (8-72) Reproduction of completed page authorized

1. Report No.	2. Government Accession No.	3. Recipient's Catalog No.
DOT/FAA/TC-25/23		

4. Title and Subtitle	5. Report Date
Implementation of Thick-Shell Finite Elements in the MAT_213 Composite Material Model in LS-DYNA	January 2026
	6. Performing Organization Code

7. Author(s)	8. Performing Organization Report No.
Ashutosh Maurya and Subramaniam Rajan	

9. Performing Organization Name and Address	10. Work Unit No. (TRAIS)
School of Sustainable Engineering and the Built Environment Arizona State University 660 South College Ave Tempe, AZ 85281-3005	Cooperative Agreement #692M152340002
	11. Contract or Grant No.

12. Sponsoring Agency Name and Address	13. Type of Report and Period Covered
Federal Aviation Administration Aircraft Certification Service Policy and Innovation Division (AIR-600) 800 Independence Avenue SW Washington, DC 20591	Final Report
	14. Sponsoring Agency Code AIR-625

15. Supplementary Notes

The FAA William J. Hughes Technical Center for Advanced Aerospace COR was Daniel Cordasco, Structures and Propulsion Branch, Aviation Research Division.

16. Abstract

One of the challenges in building a predictive numerical model for composites is accurately modeling the behavior of a structure, especially under impact loading. In prior reports, details of a newly developed orthotropic material model that has three distinct sub-models for describing deformation, damage, and failure of general composites, and has been implemented in the commercial finite element program, LS-DYNA, as *MAT_213 (*MAT_COMPOSITE_TABULATED_PLASTICITY _DAMAGE), were presented. Specifically, the prior implementations supported the use of thin shell and solid finite elements. This report discusses the implementation of thick shell elements to support the MAT_213 constitutive model in LS-DYNA as well as the verification and validation (V&V) tests carried out to ensure that the implementation is accurate and robust.

17. Key Words	18. Distribution Statement
Orthotropic plasticity, damage, fracture, explicit finite element analysis, thick shell finite element, impact simulations, composite failure, LS-DYNA, MAT_213, tabulated material model, verification, validation	This document is available to the U.S. public through the National Technical Information Service (NTIS), Springfield, Virginia 22161. This document is also available from the Federal Aviation Administration William J. Hughes Technical Center at actlibrary.tc.faa.gov.

19. Security Classif. (of this report)	20. Security Classif. (of this page)	21. No. of Pages	19. Security Classif. (of this report)
Unclassified	Unclassified	33	Unclassified

Contents

Figures

Tables

Acronyms

Acronym	Definition
CZE	Cohesive Zone Element
DIC	Digital Image Correlation
FAA	Federal Aviation Administration
FE	Finite Element
V&V	Verification & Validation

Executive summary

One of the challenges in building a predictive numerical model for composites is accurately modeling the behavior of the structure, especially under impact loading. In prior reports, details of a newly developed orthotropic material model that has three distinct sub-models for describing deformation, damage, and failure of general composites, and has been implemented in the commercial finite element program, LS-DYNA, as *MAT_213 (*MAT_COMPOSITE_TABULATED_PLASTICITY _DAMAGE), were presented. Specifically, the prior implementations supported the use of thin shell and solid finite elements. This report discusses the implementation of thick shell elements to support the MAT_213 constitutive model in LS-DYNA as well as the verification and validation (V&V) tests carried out to ensure that the implementation is accurate and robust.

1 Introduction

There are many different element types with underlying behavioral assumptions that can be used in finite element (FE) models. In this research project, test coupons and structural components subjected to quasi-static and impact loadings have been modeled with three different element types: thin shell, thick shell, and solid FEs.

Based on the ratio of thickness h to length L for any given component or structure, Akin (2010) provides some excellent guidance as shown in Figure 1. The thickness-to-length ratio, (h/L) can provide some guidance on when an element type may be appropriate to use. When (h/L) is large, transverse shear deformation in the thickness direction becomes increasingly important, requiring the use of solid elements to capture the deformations. In contrast, transverse shear deformation is negligible when (h/L) is small, and thin shell elements are probably the most efficient element choice. The thick shell elements will be the most economical in the intermediate (h/L) range.

Figure 1 shows the extensive overlap between thin and thick shells as well as thick shell and solid elements, highlighting the fact that thick shells bridge the gap between thin shells and solid elements.

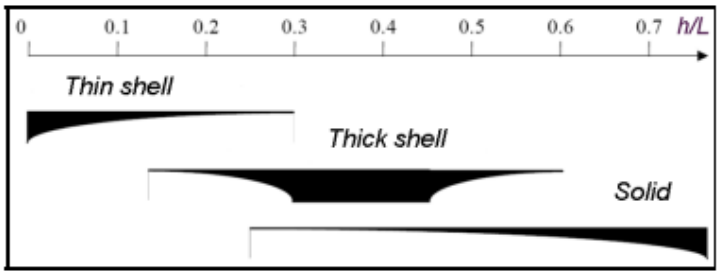

Figure 1. Overlapping valid ranges of element types

The following sections contain a summary of implementation, the material properties obtained from experiments, nine verification tests, and two validation tests. The verification tests include tension and compression tests in 1, 2 and 3 directions and shear tests in 1-2, 2-3 and 1-3 planes. The validation tests include stacked-ply compression and tension tests loaded at quasi-static loading conditions, and impact tests.

2 Implementation of thick shell finite element

LS-DYNA (LS-DYNA®, 2022) has six different element formulations for thick shell. These formulations can be divided into two types based on the constitutive models used: Type 1 and Type 2 (Figure 2).

Type 1 thick shell formulations are based on solid thin-shell constitutive models and include ELFORMs 1, 2, and 6:

- ELFORM=1 employs a one-point reduced integration scheme and is the default formulation.
- ELFORM=2 uses selective reduced integration with a 2×2 in-plane Gauss quadrature.
- ELFORM=6 uses an assumed strain reduced integration technique specifically developed for shell materials.

These Type 1 elements are based on the Reissner-Mindlin kinematic assumption involving five degrees of freedom (DOF) in the local coordinate system and results in six DOFs globally (Haufe, Schweizerhof, & Dubois, 2013). A plane stress-based constitutive law is applied, and the thickness change is governed by Poisson's ratio.

Type 2 thick shell formulations are based on solid constitutive models and include ELFORMs 3, 5, and 7:

- ELFORM=3 utilizes an assumed strain formulation with 2×2 in-plane integration.
- ELFORM=5 applies an assumed strain reduced integration method designed for brick elements.
- ELFORM=7 also uses an assumed strain formulation with 2×2 in-plane integration.

Type 2 elements use a three-dimensional constitutive law, and thickness changes arise naturally from the associated degrees of freedom.

All six thick shell element formulations are supported by MAT_213. However, only ELFORM=1 and ELFORM=5 have been used in the V&V tests as documented in this report.

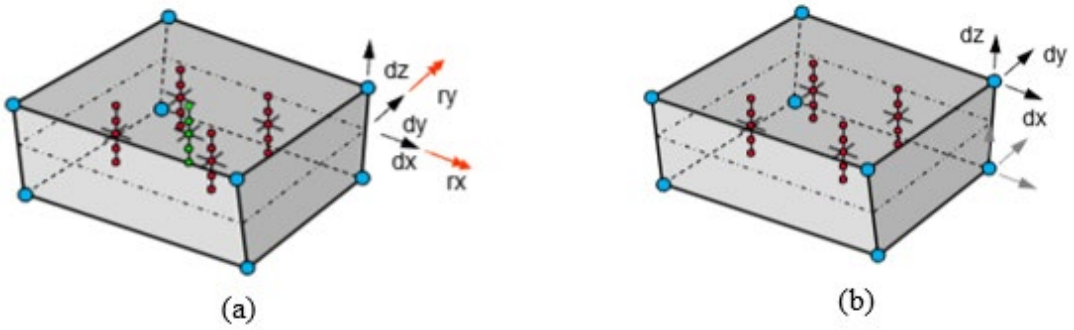

Figure 2. Thick shell element formulations- (a) Type 1, and (b) Type 2

Thick shell element in MAT_213 has been implemented in LS-DYNA in exactly the same manner as the existing implementation in MAT_213 for thin shell (for Type 1 thick shell elements) and for solid (for Type 2 thick shell elements) FEs.

3 Verification and validation test cases

Verification and validation (V&V) tests are required exercises in the development of any material model. Verification ensures that the implementation of the model has been performed correctly and adheres to its theoretical foundations. This step often begins with straightforward tests such as single-element simulations. Meanwhile, validation evaluates the accuracy, fidelity, and reliability of the developed material model by comparing its predictions against experimental data or well-established benchmarks. Together, these exercises provide confidence in the robustness and applicability of the material model. The V&V processes discussed in this section focus on a specific carbon/epoxy unidirectional composite material: T800/F3900, manufactured by Toray Carbon Fibers America (Toray, 2020). Two computing platforms were used in the V&V exercise: a Dell Precision workstation with four cores running Red Hat Linux was used to the verification tests, and Arizona State University's Sol supercomputer (Arizona State University, n.d.) using 128 cores was used for the validation tests.

3.1 Verification tests

The verification tests are carried out using T800S/F3900 composite. These tests are carried out using (a) quasi-static loading conditions, and (b) only the quasi-static room-temperature stress-

strain curves. The properties of the composite obtained from the experiments at the coupon level are listed in Table 1 and Table 2 (Khaled B. , et al., 2017). The verification tests are carried out using single element FE models initially. The single element verification model are cubes of dimension 1 in × 1 in × 1 in. (FAA Report, 2019). The FE models were created using LS-PrePost V4.9.

Table 1. Material properties

Property	**Value (Tensile)**	**Value (Compressive)**
1-direction modulus (E_{11}, psi)	23.5×10^6 (162 GPa)	18.7×10^6 (128 GPa)
2-direction modulus (E_{22}, psi)	1.07×10^6 (7.3 GPa)	1.12×10^6 (7.7 GPa)
3-direction modulus (E_{33}, psi)	9.66×10^5 (6.6 GPa)	1.04×10^6 (7.1 GPa)
1-2 plane shear modulus (G_{12}, psi)	5.80×10^5 (3.9 GPa)	
2-3 plane shear modulus (G_{23}, psi)	3.26×10^5(2.2 GPa)	
1-3 plane shear modulus (G_{13}, psi)	3.48×10^5 (2.3 GPa)	
Poisson's ratio (ν_{12})	0.317	0.342
Poisson's ratio (ν_{23})	0.484	0.728
Poisson's ratio (ν_{13})	0.655	0.578
Poisson's ratio (ν_{21})	0.0168	0.0207
Poisson's ratio (ν_{32})	0.439	0.676
Poisson's ratio (ν_{31})	0.027	0.032
Density (ρ, slugs/in^3)	1.457×10^{-4}	

Table 2. T800S/F3900 strength parameters

Component	**Ultimate strain**		**Peak stress (psi)**	
Tension 1-direction	$\left(\varepsilon_u^t\right)_{ii}$	0.01561	$\hat{\sigma}_{11}^T$	366097
Tension 2-direction	$\left(\varepsilon_u^t\right)_{ii}$	0.00622	$\hat{\sigma}_{22}^T$	6491
Tension 3-direction	$\left(\varepsilon_u^t\right)_{ii}$	0.00421	$\hat{\sigma}_{33}^T$	4002
Compression 1-direction	$\left(\varepsilon_u^c\right)_{ii}$	0.00629	$\hat{\sigma}_{11}^C$	105765
Compression 2-direction	$\left(\varepsilon_u^c\right)_{ii}$	0.04127	$\hat{\sigma}_{22}^C$	25548

Component	Ultimate strain		Peak stress (psi)	
Compression 3-direction	$\left(\varepsilon_u^c\right)_{ii}$	0.02856	$\hat{\sigma}_{33}^C$	25261
Shear 1-2 plane	$\left(\varepsilon_u\right)_{12}$	0.13316	$\hat{\sigma}_{12}$	18624
Shear 2-3 plane	$\left(\varepsilon_u\right)_{23}$	0.00428	$\hat{\sigma}_{23}$	2816
Shear 1-3 plane	$\left(\varepsilon_u\right)_{13}$	0.07015	$\hat{\sigma}_{13}$	12429

In the schematic of the single element model used, all the translational displacements are restrained either by pin or roller support. The black color arrows represent a velocity applied to the node in the corresponding direction. The green color line represents the orientation of the fiber in the composite. Stress-strain curves from different verification tests are extracted from the simulation results and are plotted with Model Curves that represent the stress-strain curves averaged over three or more test replicates.

Eight-noded thick shell elements are used with ELFORM=1 and ELFORM=5 (1-direction tension, 2-direction tension, 1-direction compression, 2-direction compression, 1-2 plane shear) and only ELFORM=5 (3-direction tension, 3-direction compression, 2-3 plane shear, 1-3 plane shear). Unless otherwise stated, the loading rate is 1 in/s.

3.1.1 1-direction tension

The schematic diagram of the model used for this simulation is shown in Figure 3. The stress-strain curves for 1-direction tension are shown in Figure 4.

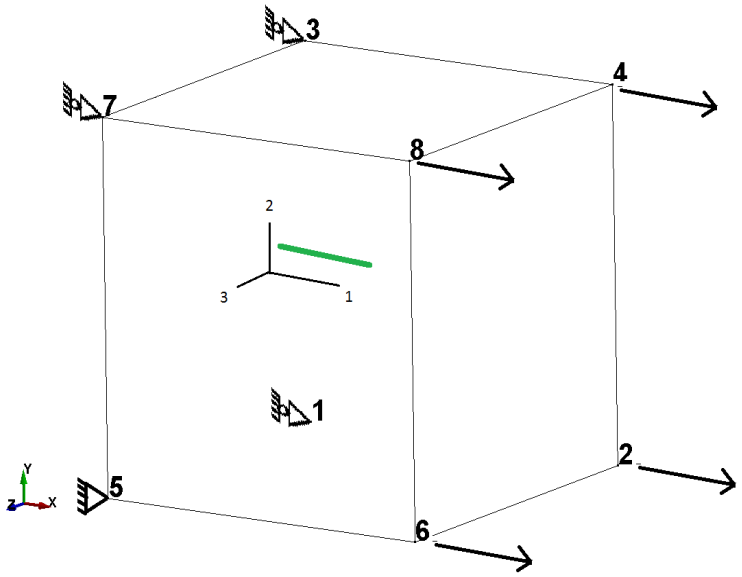

Figure 3. 1-direction tension model schematic diagram

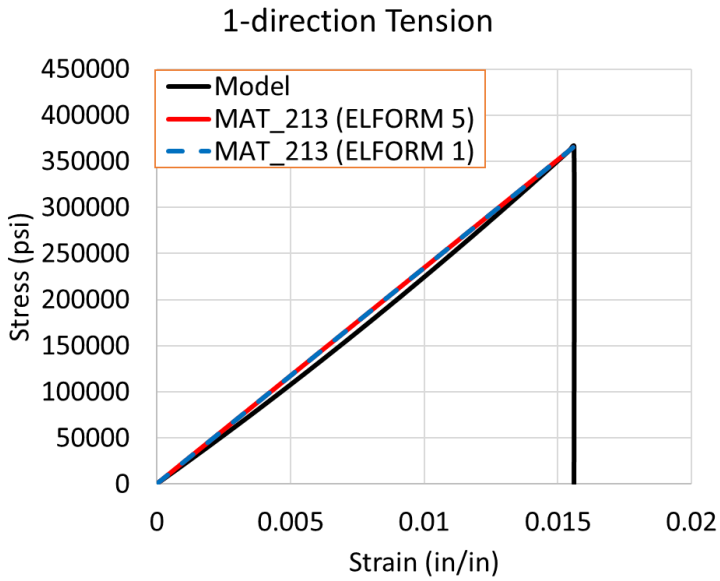

Figure 4. Stress-strain curves from 1-direction tension test with model curve

3.1.2 2-direction tension

The schematic diagram of the model used for this simulation is shown in Figure 5. The stress-strain curves for 2-direction tension are shown in Figure 6.

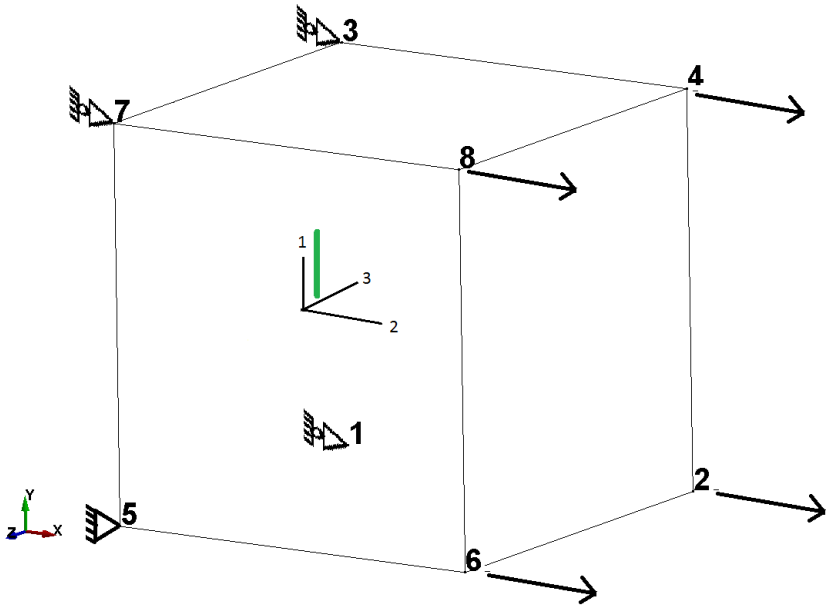

Figure 5. 2-direction tension model schematic diagram

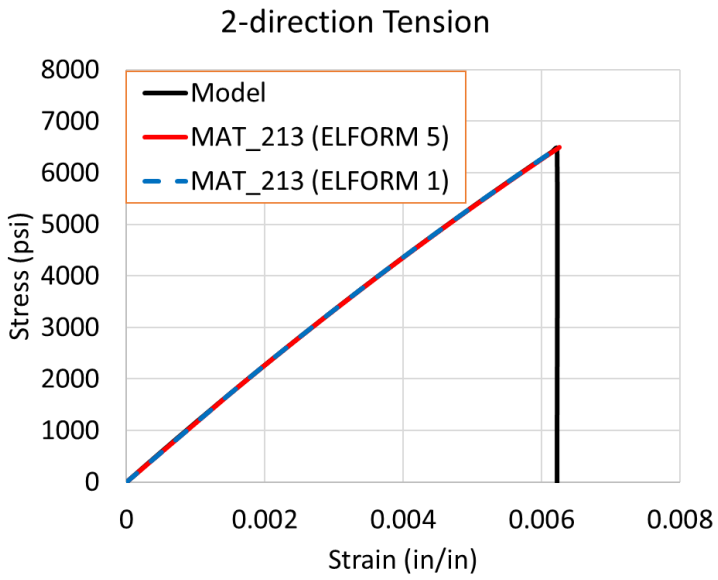

Figure 6. Stress-strain curves from 2-direction tension test with model curve

3.1.3 3-direction tension

The schematic diagram of the model used for this simulation is shown in Figure 7. The stress-strain curves for 3-direction tension are shown in Figure 8.

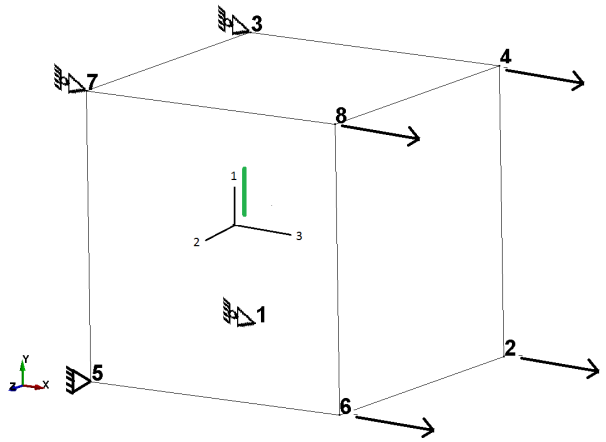

Figure 7. 3-direction tension model schematic diagram

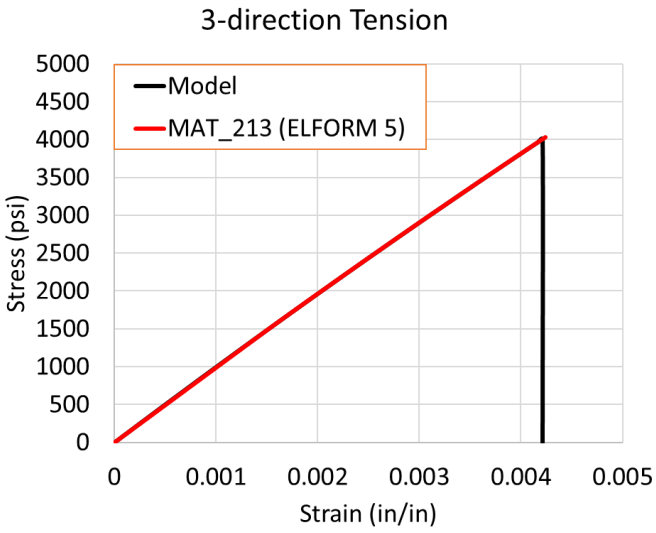

Figure 8. Stress-strain curve from 3-direction tension test with model curve

3.1.4 1-direction compression

The schematic diagram of the model used for this simulation is shown in Figure 9. The stress-strain curves for 1-direction compression are shown in Figure 10.

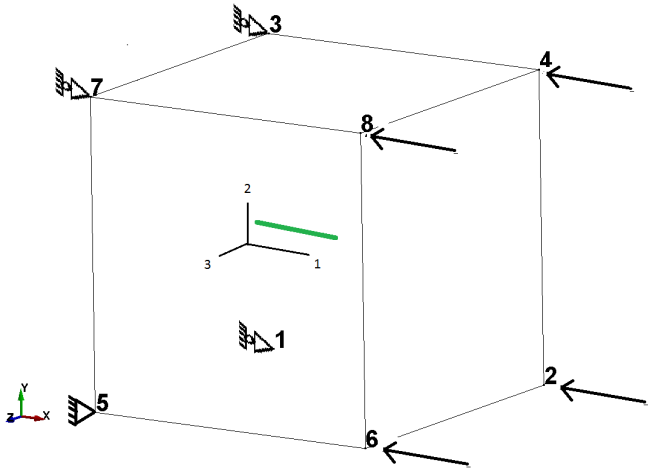

Figure 9. 1-direction compression model schematic diagram

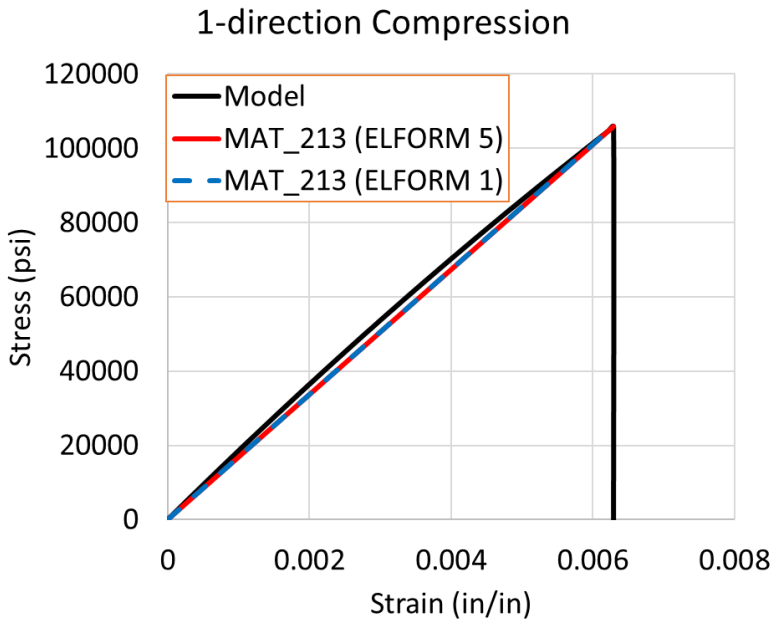

Figure 10. Stress-strain curves from 1-direction compression test with model curve

s

3.1.5 2-direction compression

The schematic diagram of the model used for this simulation is shown in Figure 11. The stress-strain curves for 2-direction compression are shown in Figure 12.

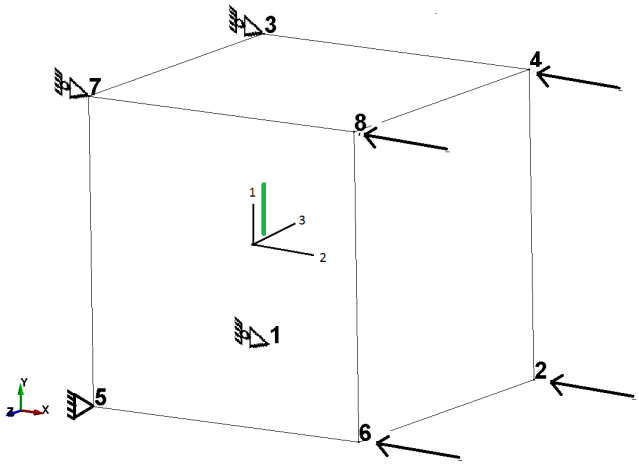

Figure 11. 2-direction compression model schematic diagram

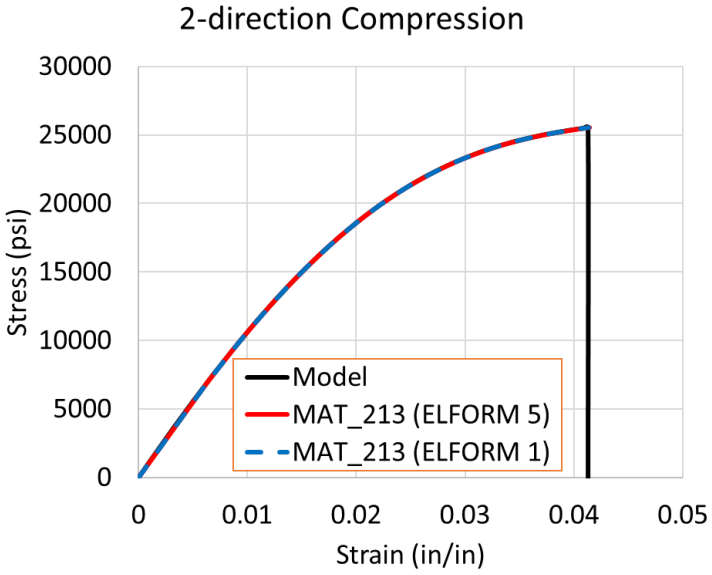

Figure 12. Stress-strain curves from 2-direction compression test with model curve

3.1.6 3-direction compression

The schematic diagram of the model used for this simulation is shown in Figure 13. The stress-strain curves for 3-direction compression are shown in Figure 14.

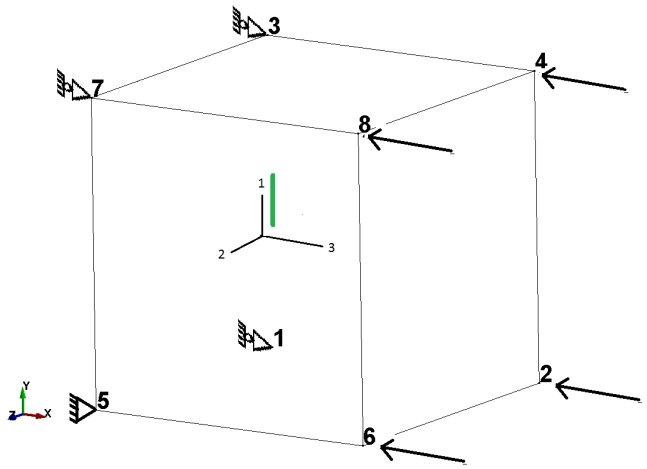

Figure 13. 3-direction compression model schematic diagram

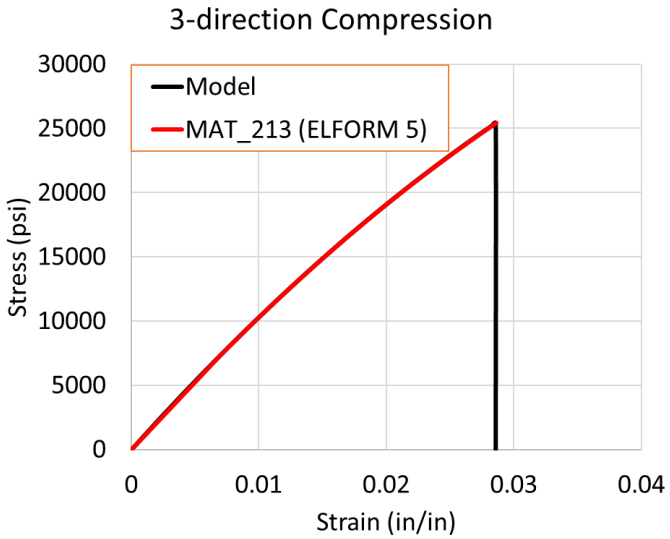

Figure 14. Stress-strain curve from 3-direction compression test with model curve

3.1.7 1-2 Plane shear

The schematic diagram of the model used for this simulation is shown in Figure 15. The stress-strain curves for 1-2 plane shear are shown in Figure 16.

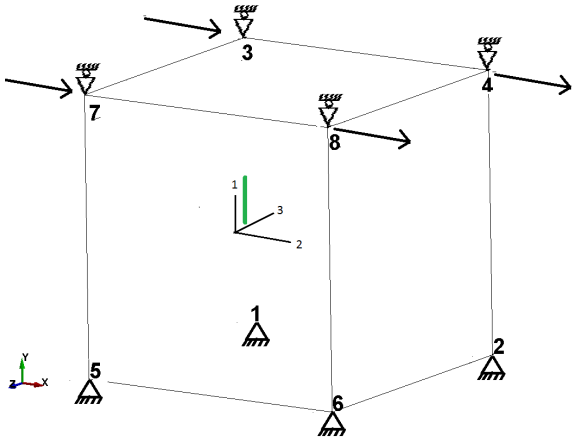

Figure 15. 1-2 plane shear model schematic diagram

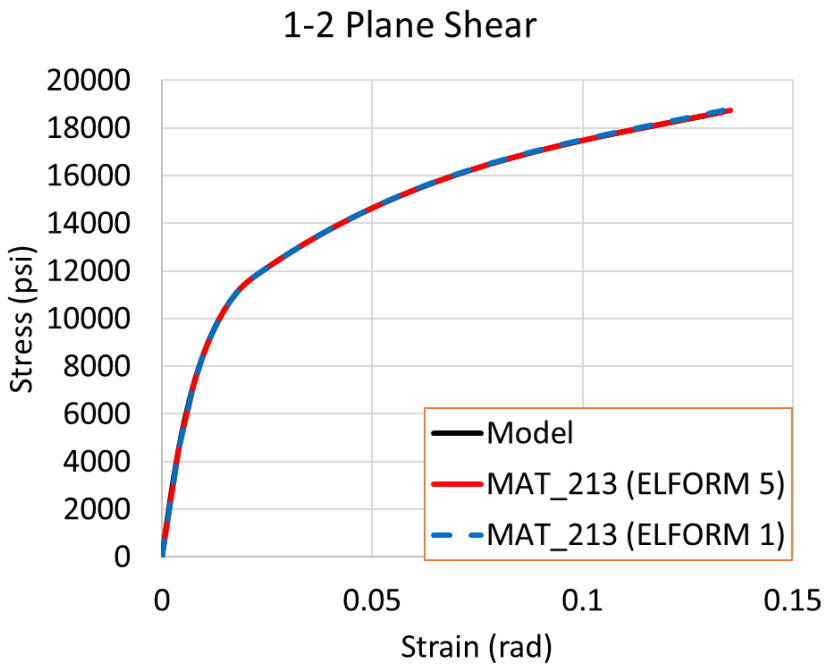

Figure 16. Stress-strain curves from 1-2 plane shear test with model curve

3.1.8 2-3 Plane shear

The schematic diagram of the model used for this simulation is shown in Figure 17. The stress-strain curves for 2-3 plane shear are shown in Figure 18.

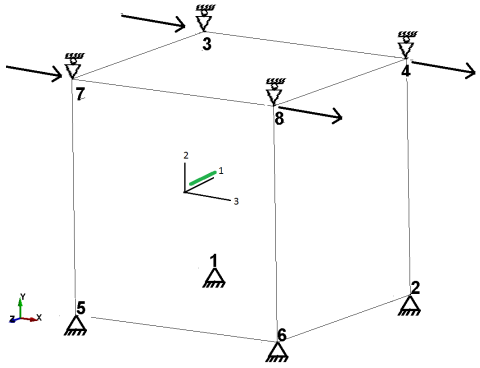

Figure 17. 2-3 plane shear model schematic diagram

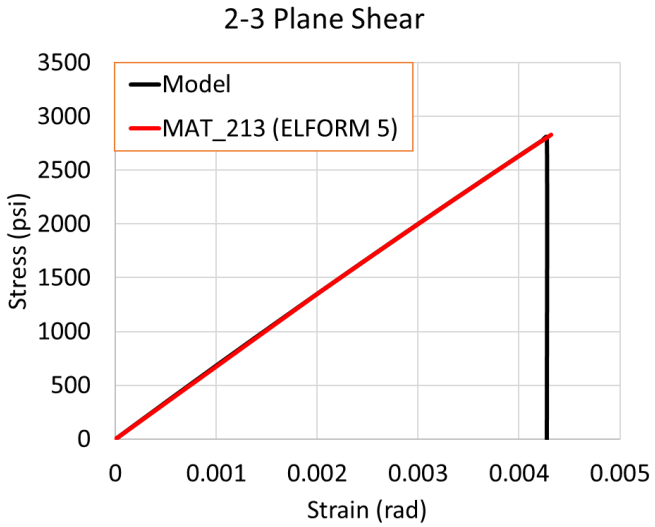

Figure 18. Stress-strain curve from 2-3 plane shear test with model curve

3.1.9 1-3 Plane shear

The schematic diagram of the model used for this simulation is shown in Figure 19. The stress-strain curves for 1-3 plane shear are shown in Figure 20.

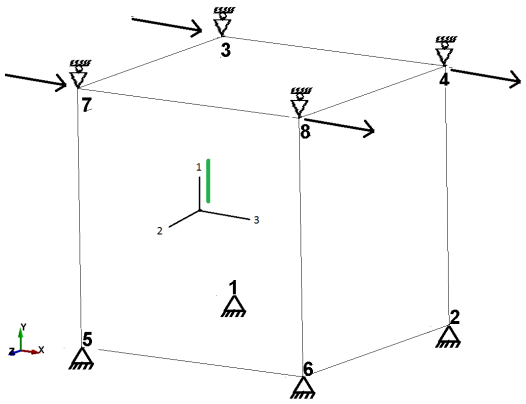

Figure 19. 1-3 plane shear model schematic diagram

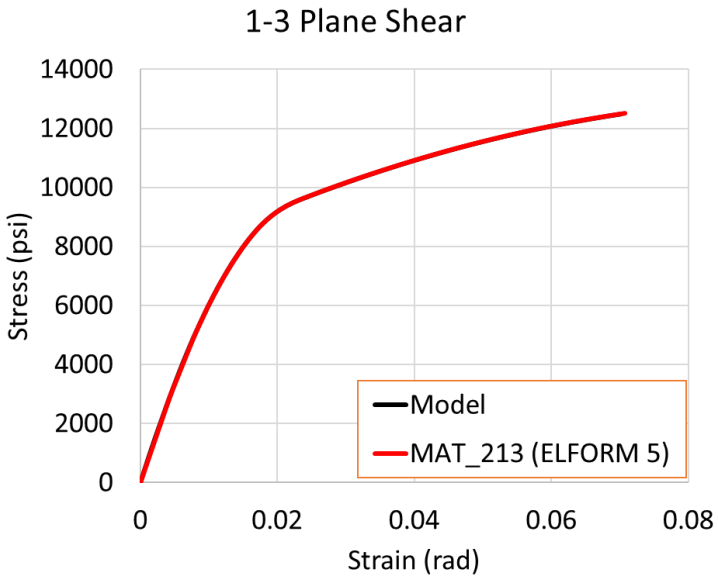

Figure 20. Stress-strain curve from 1-3 plane shear test with model curve

3.2 Validation tests

Two different validation tests were conducted. The first test is a quasi-static loading test while the second test is an impact test. In modeling both the tests, MAT_213 was used for the composite ply layers and cohesive zone elements (CZE) were modeled with MAT_186 for the interlaminar matrix. Details of the utilization of MAT_186 in combination with MAT_213 and the specific properties used for MAT_186 in this work are given in (Khaled B. M., et al., 2019; Shyamsunder, et al., 2022). The nine input curves are used as MAT_213 stress-strain input since ELFORM=5. Data from Double-Cantilever Beam and End-Notch Flexure tests (Khaled B. M., et al., 2019) were used for modeling the CZE.

3.2.1 Stacked-ply validation test

The stacked-ply validation tests model an eight-ply panel of T800/F3900 specimens with a $[0/90/+45/-45]_S$ layup. Details of the specimens are shown in Figure 21. The grey regions show where fiberglass tabs were glued to the specimen. The tabs prevent the specimens from crushing when the specimens are inserted and held in the fixtures. The white center region is the gage section that was speckled for gathering Digital Image Correlation (DIC) data. More details are available in earlier publications (Ashutosh & Rajan, 2024; Shyamsunder, Khaled, Rajan, & Blankenhorn, 2020).

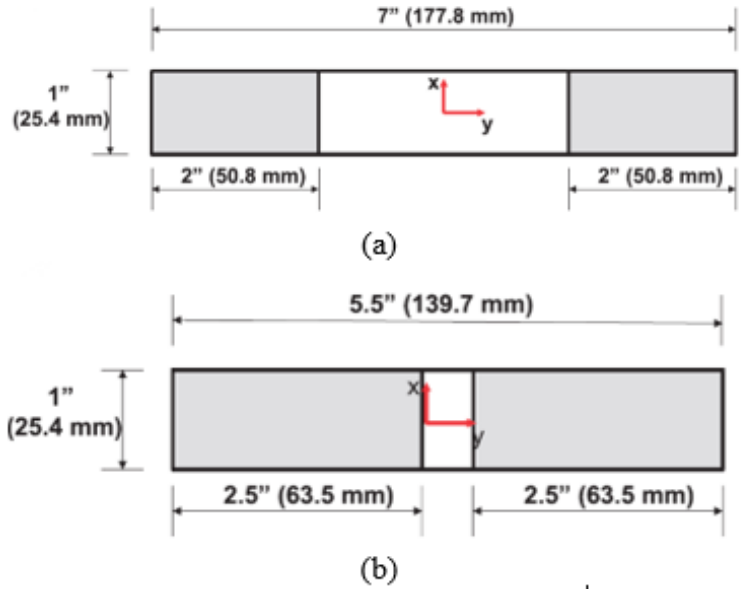

Figure 21. Schematic diagrams for stack ply validation test: (a) tension, and (b) compression

3.2.1.1 Finite element model

Only the gage section was modeled using eight-noded thick shell elements with ELFORM 1 and ELFORM 5. There are eight elements through thickness corresponding to the eight plies in the experimental specimen. CZE were used between ply layers with eight node hexahedral solid elements (ELFORM=19). Since only the gage section is modeled, the displacement at the end of the gage section from the experiment was taken from the DIC analysis (Figure 21) and applied to the FE model on the loading face nodes. Note that the loading rate has been increased by 10^4 for the tension test and 10^5 for the compression test in order to reduce the computational time. To mimic the actual laboratory tests that were conducted at quasi-static loading rate, rate-dependent stress-strain curves are not used in the simulation. Energy checks show a minimal impact on the results as kinetic energy is a small negligible fraction of the total energy.

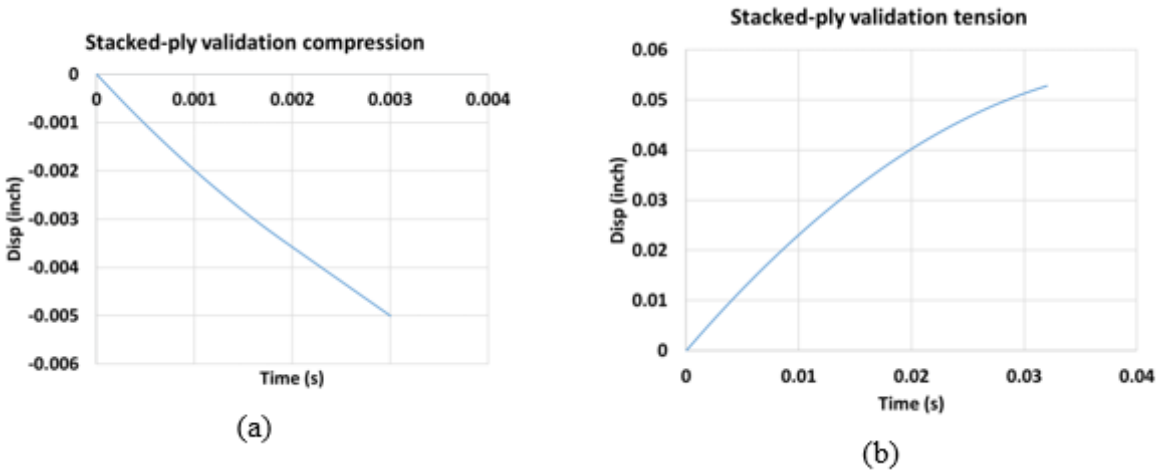

Figure 22. Load curves for stacked ply tests: (a) compression, and (b) tension

3.2.1.2 Material Data

The composite panels were modeled using MAT_213, with the Generalized Tabulated Failure Criterion (GTFC) activated. Details of the implementation and use of the damage model and the GTFC failure model are provided in (Shyamsunder, et al., Numerical validation of composite panel impact tests, 2022; Shyamsunder, Khaled, Rajan, & Blankenhorn, 2020). The post peak curve is obtained by calibration to match simulation results with the experimental results. Details are provided in Table 3.

Table 3 . MAT_213 input parameters for stacked-ply test

Model	Residual Strength	Erosion strain
Solid, ELFORM 1	10.0% (T1, T2, S12) 100% (C1, C2, C3) 10.0% (T3, S23, S13)	Tension: 0.05 Compression: 0.009
Thin shell, ELFORM 16	10.0% (T1, T2, S12) 100% (C1, C2)	Tension: 0.05 Compression: 0.02
Thick shell, ELFORM 1	10.0% (T1, T2, S12) 100% (C1, C2, C3)	Tension: 0.02 Compression: 0.0085
Thick shell, ELFORM 5	10.0% (T1, T2, S12) 100% (C1, C2, C3) 10.0% (T3, S23, S13)	Tension: 0.10 Compression: 0.02

3.2.1.3 Results

Figure 23 shows the load versus time plots for both the stacked-ply tension and compression models. The results from the thick shell element formulation are compared with those from solid elements (Shyamsunder, Khaled, Rajan, & Blankenhorn, 2020) and thin shell elements (Ashutosh, 2025; Ashutosh & Rajan, 2024). The load-time responses from the FE models of compression tests show good agreement with the experimental results. Across all four element formulations, the predicted peak loads fall within an acceptable range of the experimental peak value. After 150 s, the thin shell model shows oscillating behavior due to the initiation of 2-direction damage in the 0° ply at $t = 150\ s$.

The FE response from the tension test exhibits slightly stiffer behavior compared to the experiment, with the peak load predicted very close to the experimental value.

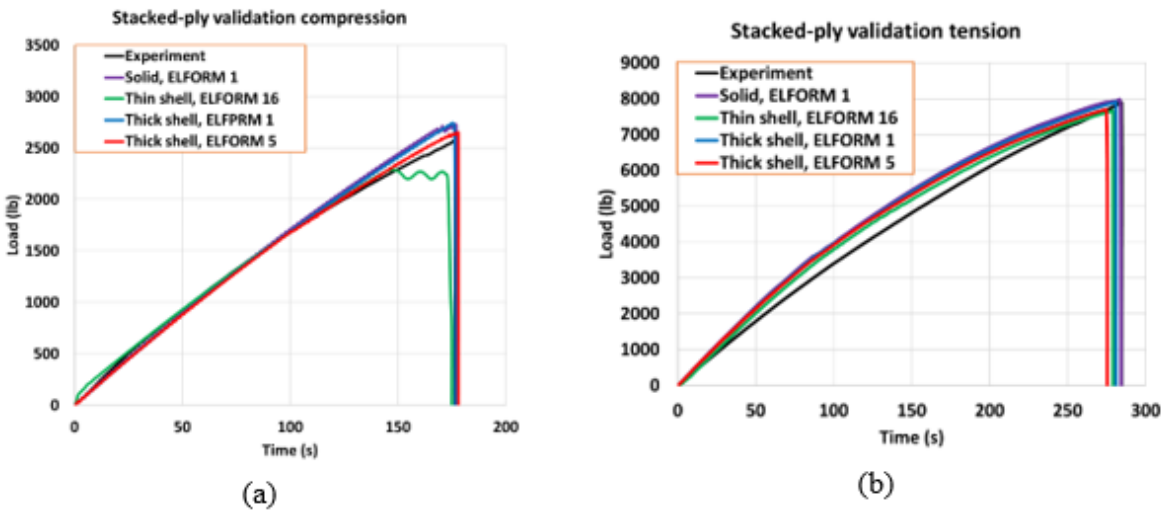

Figure 23. Stacked ply results: (a) compression, and (b) tension

3.2.2 Impact validation test

A series of impact tests were conducted at the NASA Glenn Research Center Impact Dynamics Laboratory using a single stage gas gun shown in Figure 24. The test utilizes a cup-shaped aluminum 2024 projectile and a 12 in × 12 in. composite panel (16-ply [(0/90/45/-45)2] s layup) clamped with 28 bolts between two thick metal plates. Two pairs of high-speed cameras were used to capture DIC images from the speckled composite panel both on the impacted side and

back side of the panel. The DIC data was analyzed to obtain full-field displacements and surface strains.

Figure 24. Single stage gas gun setup at NASA Glenn Research Center

In addition, two pairs of cameras were placed in front of and behind the panel to measure the projectile velocity and orientation before and after impact using photogrammetry software. Further details can be found in earlier publications (Ashutosh, 2025; Ashutosh & Rajan, 2024; Shyamsunder, et al., Numerical validation of composite panel impact tests, 2022; Shyamsunder, et al., 2022). LVG1075 is selected for the validation test because its high initial velocity of 385 ft/s is close to the ballistic limit of the composite panel. Note that the (experimental) rebound velocity is 46.4 ft/s.

3.2.2.1 Finite element model

The structural model consists only of the composite panel and the projectile. Figure 25 shows details of the 16 layers in the panel, the 28 bolt holes, and the projectile. A layer of CZE is placed between each pair of plies. 164,800 eight-noded fully integrated thick shell elements (ELFORM=5) are used to model the composite panel. 154,500 eight-noded hexahedral solid elements (ELFORM=20) form the CZE elements. There are 17,040 solid elements in the projectile. To replicate the test setup, the nodes on the circumference of the bolt holes were restrained in-plane, while the nodes at location of the bolt hole clamps at the top and bottom layers were restrained in the out-of-plane direction.

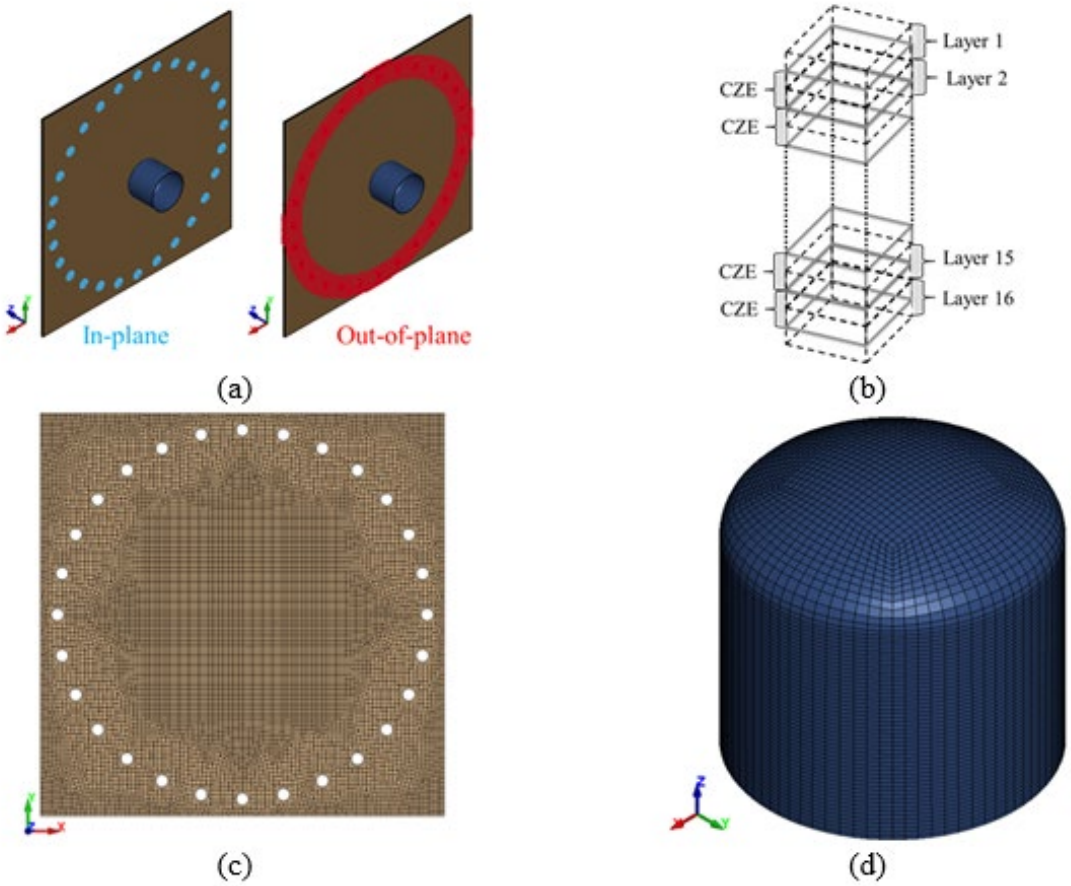

Figure 25. FE model details: (a) panel, projectile, and in-plane and out-of-plane fixity conditions; (b) close-up of typical inter-ply regions showing CZE elements; (c) panel; and (d) projectile

3.2.2.2 Material data

The composite panels were modeled using MAT_213, with the GTFC activated. The post peak curve is obtained by calibration to match simulation results with the experimental results. Details are provided in Table 4. The projectile is modeled using MAT_024 incorporating strain-rate dependent elastoplastic behavior with the data obtained from publicly available data (Nicholas, 1980).

Table 4. MAT_213 input parameters for impact test

Model	Residual Strength	Erosion strain
Solid, ELFORM 1	32.0% (T1, T2, S12) 100% (C1, C2, C3)	0.8

Model	Residual Strength	Erosion strain
	30.0% (T3, S23, S13)	
Thin shell, ELFORM 16	6.0% (T1, T2, S12) 100% (C1, C2)	0.8
Thick shell, ELFORM 5	32.0% (T1, T2, S12) 100% (C1, C2, C3) 30.0% (T3, S23, S13)	0.3

3.2.2.3 Results

This is a contained test where the projectile velocity is slightly below threshold penetration velocity. The results are shown in Figure 26. The results from the thick shell element formulation are compared with those from solid elements and thin shell elements (Ashutosh, 2025; Ashutosh & Rajan, 2024; Shyamsunder, et al., 2022). The displacement at Point 2 is accurately captured by both the solid and thick shell models, whereas the thin shell model overestimates the displacement after the first peak and fails to capture the subsequent negative peak. At Point 3, where the displacement is significantly smaller than at Point 2, the results show a varied pattern. Initially, the thick shell and solid models over predict the displacement, while the thin shell model under predicts it. However, all element formulations converge toward the experimental response during the later stages of the simulation. The final projectile velocity is predicted accurately by the thin shell model, whereas the solid and thick shell models slightly over predict it.

Table 5 presents the run time details for each simulation.

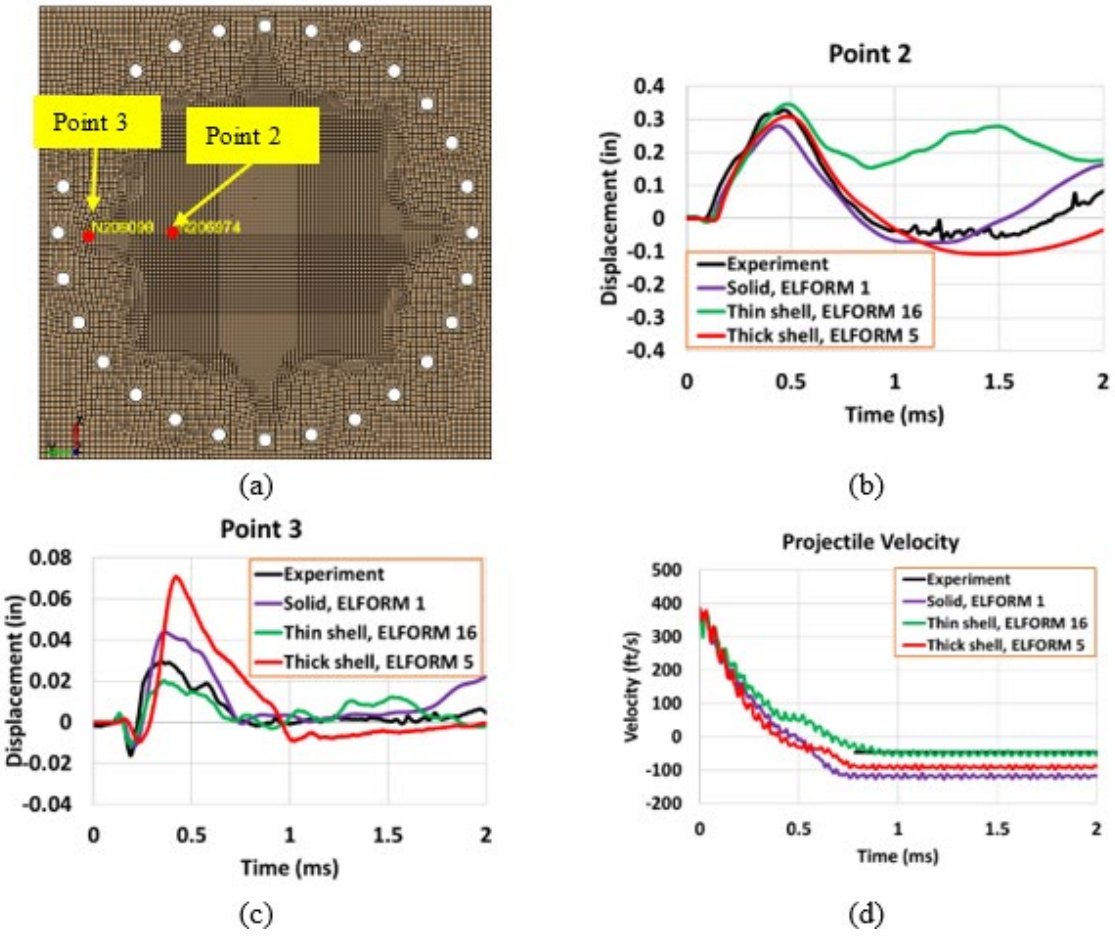

Figure 26. LVG1075 results: (a) points on the panel backside where out-of-plane displacements were monitored; (b) out-of-plane displacements at point 2; (c) out-of-plane displacements at point 3; and (d) projectile velocity

Table 5. Run time comparison for impact tests

Element Type	**Computing Platform (# Cores)**	**# of Elements**	**Wall-Clock Time (Hour:Min)**
Solid (ELFORM=1)	Sol supercomputer (128)	164800 Solid + 154500 CZE	3:50
Thin shell (ELFORM=16)		185536 Shell + 17040 Solid + 173940 CZE	3:45
Thick shell (ELFORM=5)		164800 Thick shell + 17040 Solid + 154500 CZE	3:19

4 Conclusions

The implementation and V&V evaluation of thick shell elements in LS-DYNA using the MAT_213 (Version 1.3.7) material model for the T800/F3900 unidirectional composite is documented in this report. The study conducted nine single-element verification tests and two structural-level validation tests to assess the performance, accuracy, and applicability of the implemented thick shell elements.

The implementation of thick shell elements in LS-DYNA, particularly using ELFORM=1 and ELFORM=5, demonstrates reliable performance for simulating the mechanical behavior of orthotropic composite materials such as T800/F3900 unidirectional composite. The verification tests, conducted using single-element FE models across multiple loading modes including tension, compression, and shear, show that the MAT_213 (V1.3.7) material model can capture the stress-strain response of the composite with high fidelity. Structural-level validation, including stacked-ply and high-velocity impact simulations, further supports the model's predictive capability, reinforcing the effectiveness of thick shell elements for capturing complex composite behavior at various structural scales.

5 References

Akin, J. E. (2010). *Finite Element Analysis Concepts" Via SolidWorks.* World Scientific.

Arizona State University. (n.d.). *Computing and Data Services: ASU Core Research Facilities*. Retrieved from https://cores.research.asu.edu/research-computing/capabilities

Ashutosh, M. (2025). *Point Cloud Failure Criterion for Impact Modeling of Composite Structures.* Arizona State University. William J. Hughes Technical Center. Retrieved from https://doi.org/10.21949/a3v2-ck29

Ashutosh, M., & Rajan, S. D. (2024, June 7). Incorporating point cloud failure criterion in an orthotropic visco-elastic-plastic material model. *58*(19). doi:https://doi.org/10.1177/00219983241260882

FAA. (2020). *Development of a Tabulated Material Model for Composite Material Failure, MAT213, Part 2: Experimental Tests to Characterize the Behavior and Properties of T800-F3900 Toray Composite.*

Haufe, A., Schweizerhof, K., & Dubois, P. (2013). Properties & Limits: Review of Shell Element Formulations. *LS-DYNA Developer Forum 2013.* doi:10.13140/RG.2.2.28097.35688

Khaled, B. M., Shyamsunder, L., Holt, N., Hoover, C. G., Rajan, S. D., & Blankenhorn, G. (2019, June). Enhancing the predictive capabilities of a composite plasticity model using cohesive zone modeling. *Composites Part A: Applied Science and Manufacturing, 121*, 1-17. Retrieved from https://doi.org/10.1016/j.compositesa.2019.03.001

Khaled, B., Shyamsunder, L., Hoffarth, C., Rajan, S. D., Goldberg, R. K., Carney, K. S., . . . Blankenhorn, G. (2017, September 21). Experimental characterization of composites to support an orthotropic plasticity material model. *Journal of Composite Materials, 52*(14). Retrieved from https://doi.org/10.1177/0021998317733319

LS-DYNA. (2022). *Keyword User's Manual* (Vol. 1).

Nicholas, T. (1980). *Dynamic Tensile Testing of Structural Materials Using a Split Hopkinson Bar Apparatus.* Technical Report.

Shyamsunder, L., Khaled, B., Rajan, S. D., & Blankenhorn, G. (2020, December 29). Improving failure sub-models in an orthotropic plasticity-based material model. *Journal of Composite Materials, 55*(15). Retrieved from https://doi.org/10.1177/0021998320982651

Shyamsunder, L., Khaled, B., Rajan, S. D., Pereira, J. M., DuBois, P., & Blankenhorn, G. (2022, January). Numerical validation of composite panel impact tests. *International Journal of Impact Engineering, 159*. Retrieved from https://doi.org/10.1016/j.ijimpeng.2021.104032

Shyamsunder, L., Maurya, A., Rajan, S. D., Cordasco, D., Revilock, D., & Blankenhorn, G. (2022, December). Impact simulation of composite panels for aerospace applications. *Composites Part B: Engineering, 247*. Retrieved from https://doi.org/10.1016/j.compositesb.2022.110320

Toray. (2020). Toray Composite Materials America.